KINK PROFILE IN A CURVED SPACE

T. Dobrowolski

Institute of Physics, Pedagogical University of Cracow
Podchorążych 2, 30-084 Kraków, Poland
dobrow@up.krakow.pl

(Received January 15, 2015; revised version received April 14, 2015; final version received April 28, 2015)

Sine-Gordon model reduced from 3+1 to 1+1 curved dimensions is considered. In the framework of the Bogomolny arguments, the existence of kink solutions in curved space is studied. The relaxation method is used to produce kink profiles in a curved Josephson junction.

DOI:10.5506/APhysPolB.46.1457
PACS numbers: 05.45.–a, 05.45.Yv, 47.20.Ky, 47.54.+r

1. Introduction

The experimental evidence of solitons in physical systems originated from an observation by Russell [1] of his waves of translation traveling along the Union Canal in Hermiston.

The mathematical description of solitons was introduced in 1965 by Zabusky and Kruskal [2] who demonstrated soliton behavior in the Korteweg–de Vries equation. The existence of solitons is a direct consequence of a balance between dispersive effects and nonlinearity.

Nowadays solitons appear in descriptions of physical, biological, chemical systems and other branches of science [3]. In physics, solitons appear as solutions of many models like: the sine-Gordon equation, the nonlinear Schrödinger, the Korteweg–de Vries equation and many variations of these models.

The concept of the soliton has also been extended in order to describe other solutions known as topological solitons or topological defects. The solutions of this type often appear in the field theory and condensed matter physics. Topological defects are stable against decay to trivial vacuum states due to some topological reasons. They are classified into different homotopy classes and, moreover, they preserve their form due to an infinite energy barrier that separates the distinct classes.

One of the best understood (due to its integrability) models is the sine-Gordon model. This model has found applications in the description of many physical systems [4]. The solutions of this model have been explored for many years [5].

For example, the sine-Gordon model describes propagation and generation of electromagnetic waves in the Josephson junction. The kink solution in this context describes the flux quantum propagating along the junction. The Josephson junction consists of two superconductors separated by a very thin surface of an insulator. Although the Josephson junction is a two-dimensional system, if the transverse dimension is smaller than the Josephson length, then the system can be considered as a one-dimensional system called the long Josephson junction. The most important degree of freedom that characterizes the dynamics of such a system is a gauge invariant phase difference of the many-particle wave functions which describe the superconducting electrodes that form the junction [4].

The present paper concentrates on existence of the kink solutions in the 1+1 sine-Gordon model defined on the curved manifold. The model considered here is obtained by dimensional reduction of the sine-Gordon model from 3+1 to 1+1 dimensions. The usefulness of this procedure was motivated in paper [6]. This paper shows that for slowly varying curvatures,s the appropriate 1+1 dimensional model correctly describes curved Josephson junctions. The studies of the influence of the nontrivial shape of the Josephson junction on the kink motion were also undertaken in papers [7–9].

2. Bogomolny analysis

The Lagrangian of the sine-Gordon model defined on the curve has the following form (see [6]):

$$\mathcal{L} = \tfrac{1}{2}\,(\partial_t\phi)^2 - \tfrac{1}{2}\,\mathcal{F}(\partial_s\phi)^2 - V(\phi)\,, \tag{1}$$

where the function $\mathcal{F}(s)$ contains information about the curvature of the considered space

$$\mathcal{F}(s) = \frac{1}{aK(s)}\,\ln\left[\frac{2+aK(s)}{2-aK(s)}\right]\,. \tag{2}$$

Here, $K(s)$ is the curvature of the central curve of the isolating layer. In a natural way, the above Lagrangian

$$L = \int\limits_{-\infty}^{+\infty} ds\,\mathcal{L} = E_{\rm k} - E_{\rm p}\,, \tag{3}$$

separates into kinetic

$$E_{\mathrm{k}} = \frac{1}{2} \int\limits_{-\infty}^{+\infty} ds (\partial_t \phi)^2 \,, \tag{4}$$

and potential energy

$$E_{\mathrm{p}} = \frac{1}{2} \int\limits_{-\infty}^{+\infty} ds \left[\mathcal{F} (\partial_s \phi)^2 + 2V(\phi) \right] \,. \tag{5}$$

One could expect that existence of the static kink solutions can be showed without invoking the equation of motion that follows from the Lagrangian density (1). Actually, static kinks are minimals of the potential energy E_{p} and their existence can be justified directly by means of the Bogomolny argument. According to the Bogomolny idea, the potential energy can be extracted as a part of the nonnegative expression

$$0 \leq \frac{1}{2} \int\limits_{-\infty}^{+\infty} ds \left| \sqrt{\mathcal{F}} \partial_s \phi \pm \sqrt{2V(\phi)} \right|^2 \,. \tag{6}$$

From the above expression, one can estimate the potential energy

$$E_{\mathrm{p}} \geq \left| \int\limits_{-\infty}^{+\infty} ds \sqrt{2V(\phi)\mathcal{F}} \; \partial_s \phi \right| = \left| \int\limits_{-\infty}^{+\infty} ds \, \frac{\delta G}{\delta \phi} \; \partial_s \phi \, \sqrt{\mathcal{F}} \right| \,, \tag{7}$$

where we introduced the superpotential G: $\frac{\delta G}{\delta \phi} \equiv \sqrt{2V(\phi)}$. In fact, the only difference between the standard Bogomolny inequality and our expression lies in the presence of the square root of the curvature-dependent function $\mathcal{F}$. As a matter of fact, this function, in a physically accessible regime, is $\sqrt{\mathcal{F}} \geq 1$ (see Fig. 1 (a)) and, therefore, one can obtain an estimation of the potential energy which is identical to the original Bogomolny inequality for the sine-Gordon model

$$E_{\mathrm{p}} \geq \left| \int\limits_{-\infty}^{+\infty} ds \, \frac{\delta G}{\delta \phi} \; \partial_s \phi \, \sqrt{\mathcal{F}} \right| \geq \left| \int\limits_{-\infty}^{+\infty} ds \, \frac{\delta G}{\delta \phi} \; \partial_s \phi \right| \,. \tag{8}$$

The reason why, in the considered context of the Josephson junction, only the interval [0,2) is physically interesting is explained in Fig. 1 (b). We presume that the thickness of the dielectric layer is constant. One can see

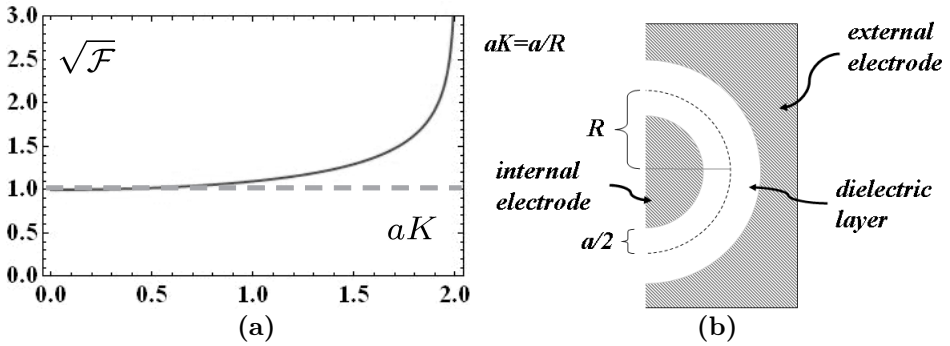

Fig. 1. (a) The square root of $\mathcal{F}$ as a function of curvature aK. (b) The transverse cross section of the Josephson junction. The gray regions represent superconducting electrodes. The electrodes are separated by the dielectric layer (white region). The thickness of the dielectric layer is denoted by a. The dashed line represents the transverse cross section of the central surface of the junction. The curvature radius of the junction is denoted by R.

that for $aK < 2$, we have two superconducting electrodes. For $aK = 2$, the internal electrode disappears. Formula (8) provides a simple estimation of the potential energy stored in the static field configurations

$$E_{\mathrm{p}} \geq \left| \int_{-\infty}^{+\infty} ds(\partial_s G) \right| = |G(\phi(+\infty)) - G(\phi(-\infty))| \,. \tag{9}$$

Let us notice that formula (9) shows that the potential energy stored in the static configuration is bounded from below, it motivates the existence of the static solutions. Moreover, as the kinetic energy is positive, the same argument holds for time-dependent configurations. The particular status in the presented argumentation has the second inequality in formula (8). Let us notice that equality at this position has a special status, it is satisfied only in the case of flat space ($\mathcal{F} = 1$). If we have a nonzero curvature, then the inequality is sharp and therefore we obtain

$$E_{\mathrm{p}} > |G(\phi(+\infty)) - G(\phi(-\infty))| \,.$$

On the other hand, the sine-Gordon potential,

$$V(\phi) = 1 - \cos\phi = 2\sin^2\frac{\phi}{2}\,, \tag{10}$$

enables explicit determination of the superpotential G

$$\frac{\delta G}{\delta \phi} \equiv \sqrt{2V(\phi)} = 2\sin\frac{\phi}{2}\,. \tag{11}$$

Integration of the last formula with respect to the field variable gives

$$G = C - 4\cos\frac{\phi}{2}\,. \tag{12}$$

In order to ensure that the field configuration has finite energy, one imposes the appropriate boundary conditions which correspond to different ground states of the potential. In dynamically different sectors of the model, they have varied forms. For example, in the sector that contains a trivial vacuum solution, the boundary conditions are the following $\phi(\pm\infty) = 0$ ($E_{\mathrm{p}} \geq 0$). On the other hand, in the sector that contains the simplest static kink solution, we have $\phi(-\infty) = 0$, $\phi(+\infty) = 2\pi$, and therefore the potential energy is limited as follows $E_{\mathrm{p}} \geq 8$. For any kink solution, without loss of generality, we can presume $\phi(-\infty) = 0$ and $\phi(+\infty) = 2\pi n$. In this case, from formulas (8) and (11), one can obtain

$$E_{\mathrm{p}} \geq 8|n|\,,$$

where we invoked the fact that the range of integration n times cover the interval $[0, 2\pi]$. We also used periodicity of the integrated function. The integer number n measures the topological charge of the field configuration

$$Q = \frac{1}{2\pi}\int\limits_{-\infty}^{+\infty} ds\ \partial_s\phi = \frac{\phi(+\infty) - \phi(-\infty)}{2\pi} = n\,.$$

Now, let us turn to Bogomolny equations which follow from the inequality (6). These equations correspond to saturation of the lower bound of this inequality

$$\sqrt{\mathcal{F}}\partial_s\phi \pm \sqrt{2V(\phi)} = 0\,. \tag{13}$$

If this equation is satisfied, then inequality (7) is saturated. In spite of the equation of motion, this equation is a first order in space variable and, therefore, is easily integrable. The solution of equation (13) has a simple form

$$\phi(s) = 4\arctan e^{f(s)}\,, \tag{14}$$

where

$$f(s) = \pm\int ds\ \mathcal{F}^{-\frac{1}{2}}\,. \tag{15}$$

It can be easily checked whether or not this solution fulfills the equation of motion

$$\partial_t^2\phi - \partial_s\left(\mathcal{F}\partial_s\phi\right) + \sin\phi = 0\,. \tag{16}$$

In the static case, the field equation (16) can be written in the form

$$\partial_s \left(\mathcal{F}\partial_s\phi\right) = \frac{\delta V}{\delta\phi}\,, \tag{17}$$

where we denoted

$$\frac{\delta V}{\delta\phi} = \sin\phi\,.$$

On the other hand, if we multiply both sides of the Bogomolny equation (13) by the square root of the function $\mathcal{F}$

$$\mathcal{F}\partial_s\phi = \pm\sqrt{2V\mathcal{F}}\,, \tag{18}$$

and next, we differentiate it with respect to space variable s, then we obtain

$$\partial_s \left(\mathcal{F}\partial_s\phi\right) = \pm\frac{1}{\sqrt{2V}}\frac{\delta V}{\delta\phi}\;\partial_s\phi\;\sqrt{\mathcal{F}} \pm \sqrt{2V}\;\partial_s\left(\sqrt{\mathcal{F}}\right)\,. \tag{19}$$

If we apply the Bogomolny equation (13) for a second time, then the first term of the last formula simplifies considerably

$$\partial_s \left(\mathcal{F}\partial_s\phi\right) = \frac{\delta V}{\delta\phi} \pm \sqrt{2V}\;\partial_s\left(\sqrt{\mathcal{F}}\right)\,. \tag{20}$$

Comparing the equation of motion (17) with equation (20), we find out that the solutions of the Bogomolny equation (13) are solutions of the equation of motion only in the case of constant curvature *i.e.* for $\partial_s\mathcal{F} = 0$. In this particular case, the kink has the same profile-like kink in flat space but its thickness is magnified by the curvature-dependent factor $1/\sqrt{\mathcal{F}}$, see equations (14) and (15)

$$\phi(s) = 4\arctan e^{\pm\frac{1}{\sqrt{\mathcal{F}}}(s-s_0)}\,.$$

Let us notice that we use dimensionless space and time variables. In the context of the Josephson junction, the space variable is measured in the units of the Josephson length λ_{J} and the time is measured in the units of the inverse plasma frequency $\omega_{\mathrm{P}} = \frac{\bar{c}}{\lambda_{\mathrm{J}}}$ (where $\bar{c}$ is Swihart velocity). In the case of conventional superconductors, the Josephson length is typically kept in the range of $10^3 \div 10^5$ nm [4, 10]. On the other hand, the typical length of the fabricated junctions belongs to the interval from zero to several hundred of λ_{J}. Actually, the junctions with the length exceeding a dozen or so Josephson units are considered as long Josephson junctions. Moreover, the Josephson length depends on the temperature of the system through the Josephson critical current and the London penetration depths of the superconducting electrodes. This dependence is responsible for unlimited increase of the Josephson penetration depth λ_{J} when the temperature approaches the critical temperature [4]. In this case, the long Josephson junction (for low temperatures) becomes a point junction (for higher temperatures).

The studies performed in this section refer to the sine-Gordon model in the unlimited space. In fact, in the mentioned context of the Josephson junction, the space is limited to the fine interval specified by the length of the junction. In fact, the simulations performed in the next section better approximate the real junction than the results presented above. All simulations were performed on the interval $[-40, 40]$. Moreover, the presumed boundary conditions with high accuracy are equal to asymptotic values $\phi(t, x = -40) = 0$ and $\phi(t, x = 40) = 2\pi$. These conditions fix the sector of the model to unit topological charge and make one-soliton solutions most preferable.

3. The kink profiles for nonconstant curvatures

The profiles of the kink solutions could be found for arbitrary nonconstant curvatures in a simple numerical way. First, we observe that the static solutions of the two-field models that differ by the dissipation term are identical and, therefore, we can add to the equation of motion the dissipation term without any influence on the static sector of the model. In the second step, we choose some initial configuration which satisfies the appropriate boundary conditions and (according to intuition) is close to the demanded solution. Finally, we wait a sufficiently long time. The initial configuration, due to dissipation, loses surplus energy and, therefore, it evolves in the direction of the static solution. This recipe is known, in literature, as the relaxation method [11].

3.1. Example 1

First, we consider the sine-Gordon model in flat space (in this case, we denote the space variable by $s = x$)

$$\partial_t^2 \phi(x,t) - \partial_x^2 \phi(x,t) + \sin\phi(x,t) = 0\,. \tag{21}$$

We introduce to the field equation (21) the dissipation term

$$\partial_t^2 \phi(x,t) + \gamma \partial_t \phi(x,t) - \partial_x^2 \phi(x,t) + \sin\phi(x,t) = 0\,. \tag{22}$$

Preparing this example at the beginning, we pretend that we do not know the exact kink solution of the considered model. Next, we choose initial data that, according to our intuition, is close to the kink solution (it also satisfies appropriate boundary conditions for the kink)

$$\phi(x,0) = 4\arctan(e^x) + 4\, e^{-\frac{1}{4}x^2}\cos x\,, \tag{23}$$

$$\partial_x \phi(x,0) = \frac{2}{\cosh x} - 2e^{-\frac{1}{4}x^2}(\cos x + 2\sin x)\,. \tag{24}$$

Let us notice that the second term in equations (23) and (24) means that this initial condition does not coincide with the exact kink solution. This term was introduced to the initial condition because we want to show that although the initial configuration is not the exact solution, the final configuration really coincides with the searched kink.

Finally, we perform simulation of the evolution of the initial configuration. The initial configuration $\phi(x, t = 0)$ and its gradient $\partial_x\phi(x, t = 0)$ are presented in Figs. 2 (a) and (b). The final configuration and its gradient are presented in Figs. 2 (c) and (d). The final configuration is compared with the kink solution $\phi_{\mathrm{K}}(x, t) = 4\arctan(e^{x-1.8})$ which is represented by a gray dashed line. Figures 2 (c) and (d) show excellent agreement of the obtained field configuration with exact kink solution of the model *i.e.* ϕ_{K}. Although the final configuration coincides with the kink profile, the position of the static kink $s_0 = 1.8$ is out of control and is solely determined by the choice of the initial field configuration. This fact is closely related to the translational invariance of the system.

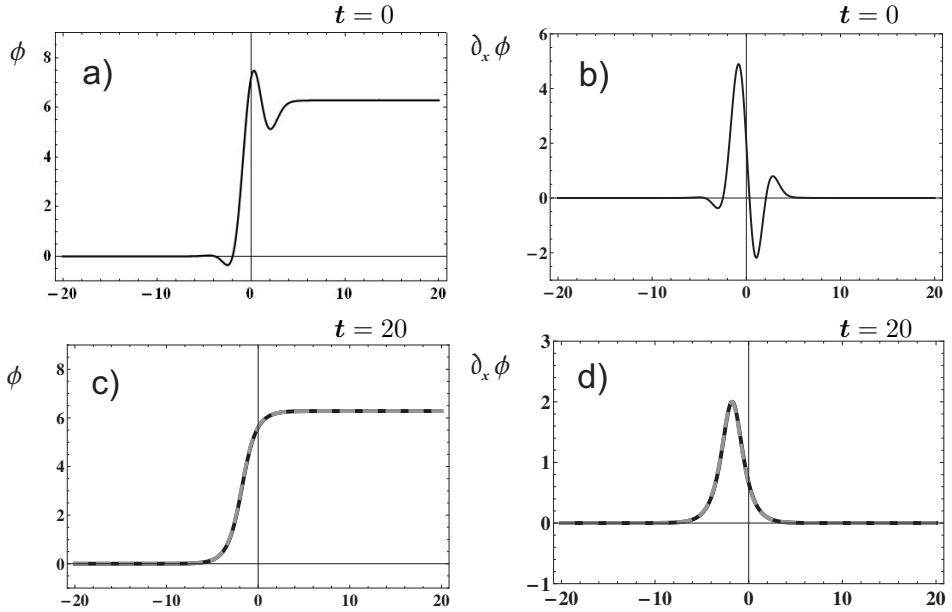

Fig. 2. (a) The initial kink configuration. (b) The space gradient of the field at instant $t = 0$. (c) The final field configuration (black line) compared with the kink located at $s_0 = 1.8$ (dashed gray line). (d) The space gradient of the field (black line) at instant $t = 20$ compared with the gradient of the kink configuration located at $s_0 = 1.8$ (dashed gray line). The dissipation constant in the simulation is $\gamma = 1$.

3.2. Example 2

Similarly, we can perform simulation for the sine-Gordon model in a curved space

$$\partial_t^2\phi(s,t) - \partial_s\left(\mathcal{F}(s)\partial_s\phi(s,t)\right) + \sin\phi(s,t) = 0\,. \tag{25}$$

We introduce to the field equation the dissipation term

$$\partial_t^2\phi(s,t) + \gamma\partial_t\phi(s,t) - \partial_s\left(\mathcal{F}(s)\partial_s\phi(s,t)\right) + \sin\phi(s,t) = 0\,. \tag{26}$$

This time, we really do not know the exact static solution of the field equation (26). We chose the initial configuration in the form characteristic for the kink solution in the flat space, see Figs. 3 (a) and (b) *i.e.*

$$\phi(s,0) = 4\arctan(e^s)\,, \qquad \partial_s\phi(s,0) = \frac{2}{\cosh s}\,. \tag{27}$$

This configuration (27) satisfies appropriate boundary conditions and therefore seems to be close to the unknown kink profile in a curved space. The

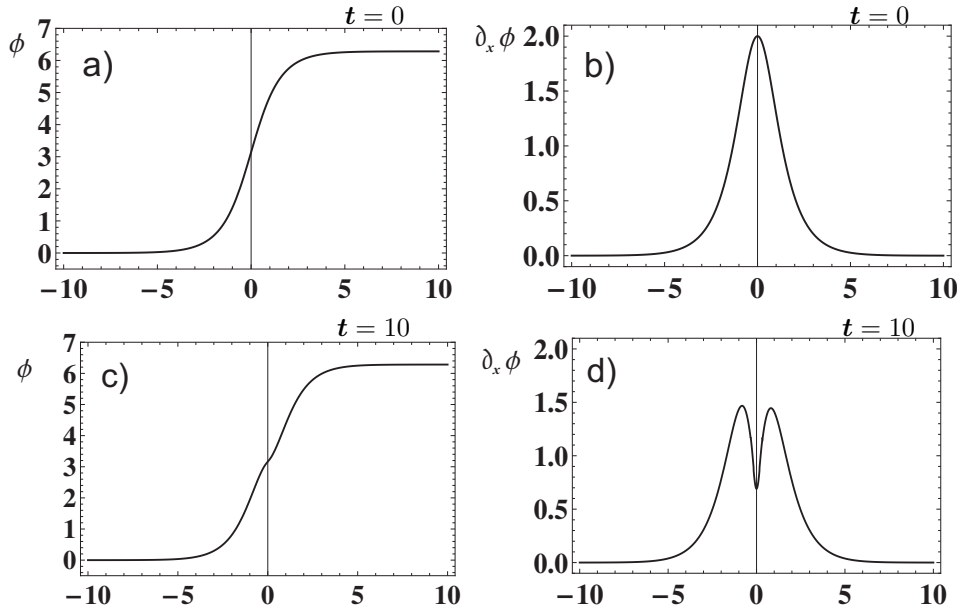

Fig. 3. Evolution of the initial configuration in a curved space. (a) The field configuration at $t = 0$. (b) The spatial derivative of the initial profile. (c) The final kink configuration in a curved space. (d) The derivative of the final field configuration (at $t = 10$). In the simulation, we presumed $\gamma = 5$.

simulation is performed for the following curvature

$$aK(s) = \frac{B}{(1+s^2)^{3/4}}\,, \tag{28}$$

where $B = 1.9999$. The final configuration is presented in Figs. 3 (c) and (d). We can see that the deformation of the kink profile has a local character and is strictly connected with the region of the nonzero curvature.

4. The kink dynamics

The dynamics of the kinks in the model (25) can also be found numerically. The curvature in performed simulation has the form (28). Depending on the initial speed of the kink and the value of the parameter B, we observe transition or reflection of the kink from the curved region.

In Fig. 4, we see interaction of the kink with the curved region of the space. The curvature of the space is represented by gray peak located in the origin of the coordinate system. These figures compare the profile of the kink that moves in a curved space (black contour) with the profile of

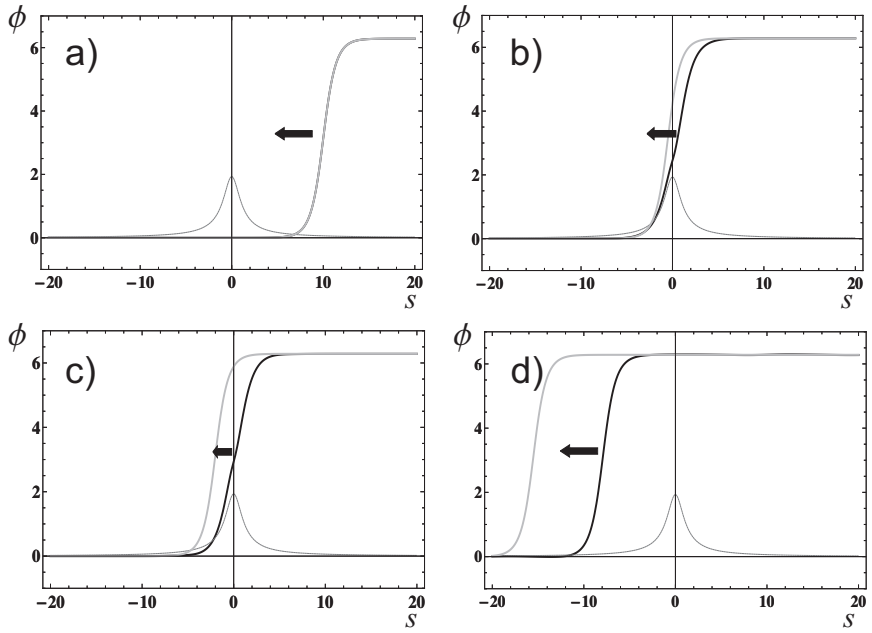

Fig. 4. Transition of the kink through the curved region of the space. The initial position and the speed of the kink are $s_0 = 10$ and $v = 0.5$. The curvature parameter in the simulation is equal to $B = 1.93$. During the propagation through the curved region of the space, the kink profile is modified and its speed is reduced.

the kink that moves in a flat space (gray contour). At the beginning, both kinks coincide. The "black" kink starts to change its profile and the speed of propagation in the curved region of the space. After interaction, sufficiently far from the curved region, kinks move almost with the same velocity.

The same process is presented in Fig. 5. This time, the figures present the space derivatives of the field ϕ and, therefore, kinks are represented by peaks. In the first figure, the profiles coincide. In the next, one can observe deformation of the profile and the change of speed of the black contour. In the last figure, we have two peaks that freely move in the same direction.

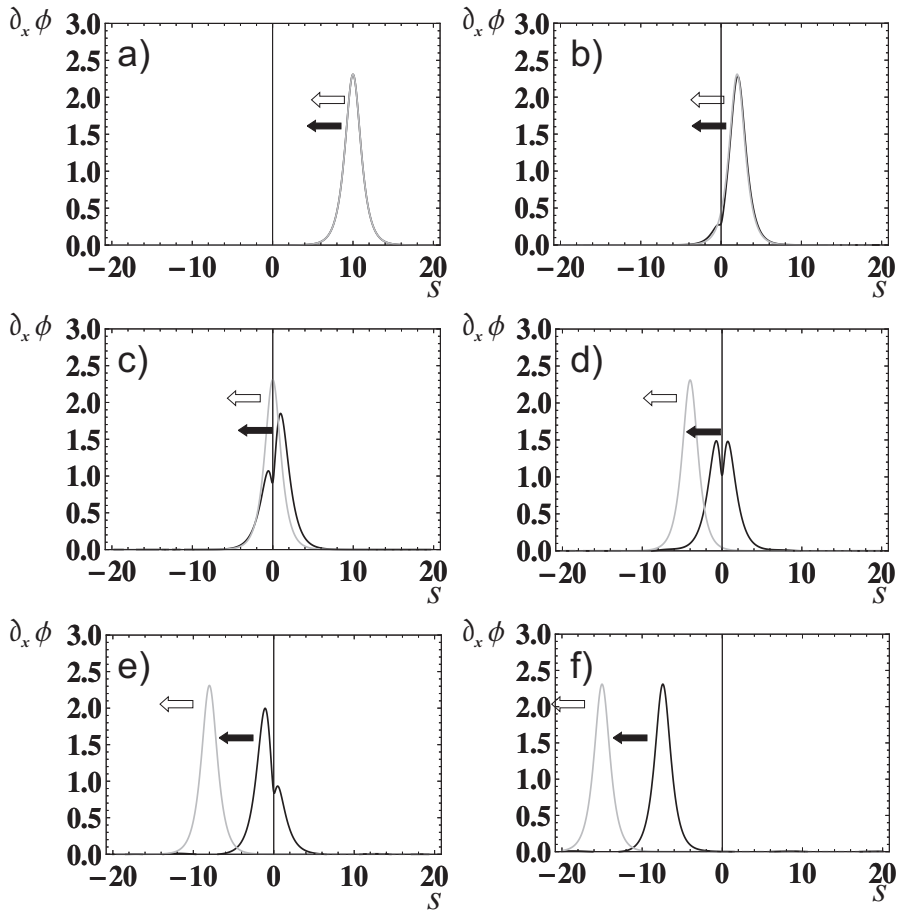

Fig. 5. The gradients of the field configuration in the process of transition of the kink through the curved region of the space. The parameters of the simulation are as follows: $B = 1.93$, $v = 0.5$, $s_0 = 10$.

The same process in the case of high velocity of the kink leads to formation of the shock wave that moves in the direction opposite to the direction of the moving kink (see Fig. 6).

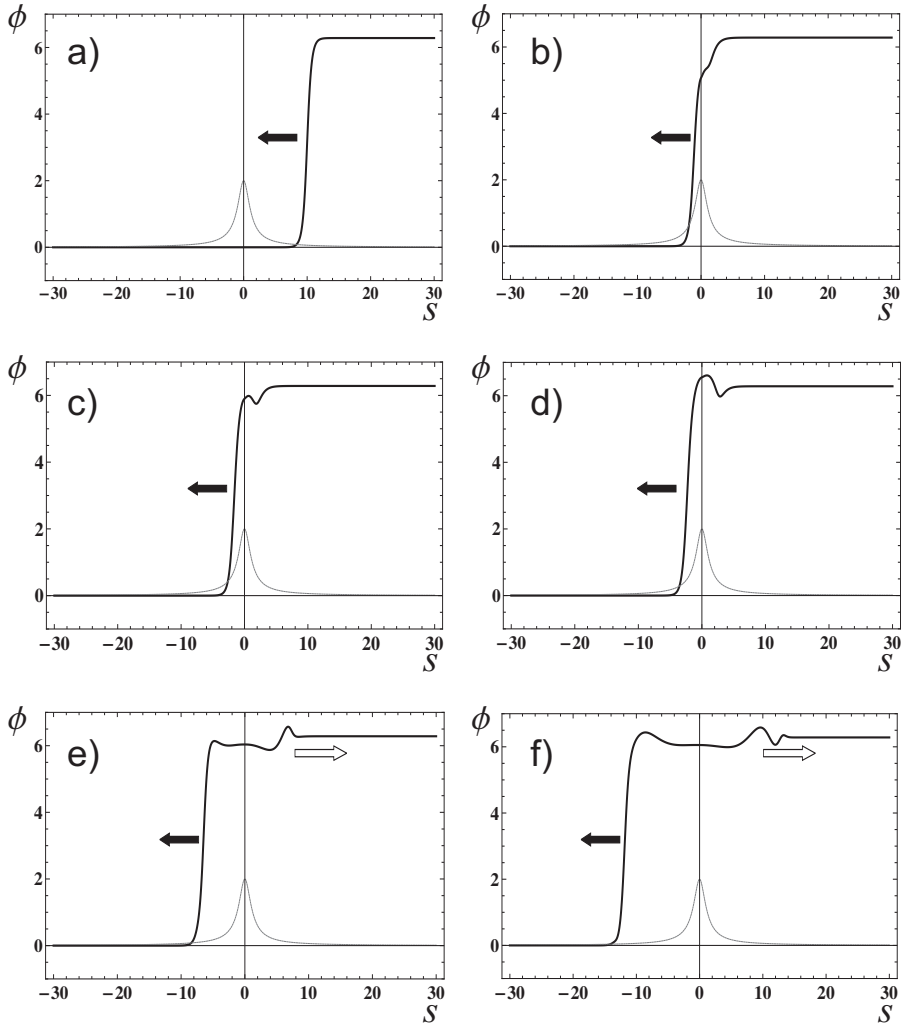

Fig. 6. Formation of the shock wave during the transition of the kink through the curved region of the space at high velocity. In the simulation, we presumed: $B = 1.999$, $v = 0.9$, $s_0 = 10$.

On the other hand, if the initial speed of the kink is sufficiently small, then the kink stops and then starts to move backward *i.e.* the kink is reflected from the curved region (see Fig. 7).

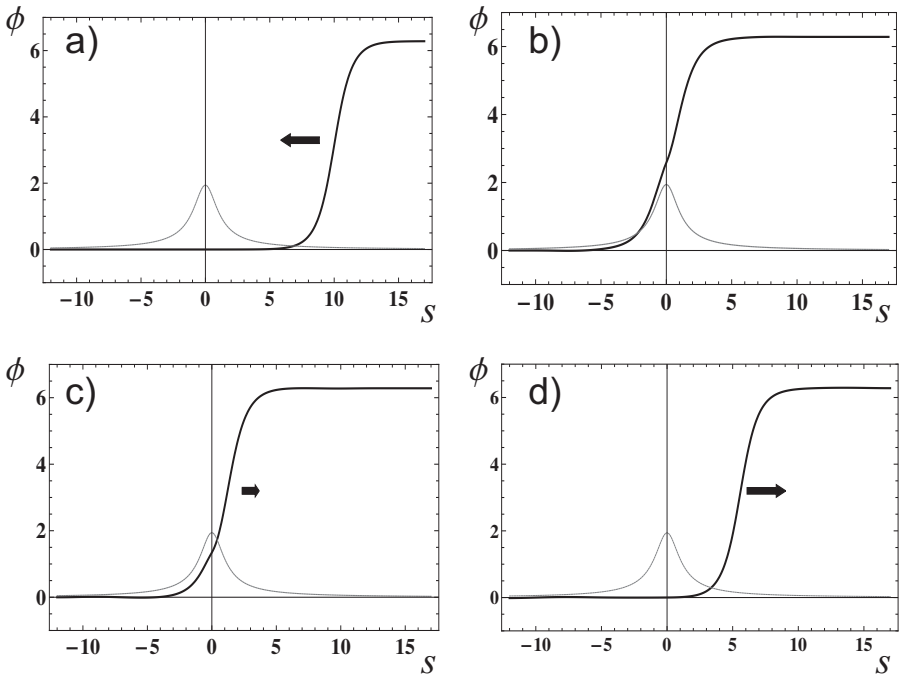

Fig. 7. Reflection of the kink from curved region. In the simulation, we took $B = 1.94$, $v = 0.5$, $s_0 = 10$.

Figure 8 shows how the kink can be trapped between two curved regions of the space. The curvature (represented by a gray contour) has the form

$$aK(s) = C\left(\frac{1}{(1+(s-l)^2)^{3/4}} + \frac{1}{(1+(s+l)^2)^{3/4}}\right). \tag{29}$$

The figure presents the gradient of the field configuration (black contour) and, therefore, the kink is represented by the peak. Although curvatures of both regions are identical, the kink, during interaction with the first curved region, radiates some part of the energy and, therefore, has not enough speed to overcome the second curved region. Moreover, when the kink comes back to the first curved region, it does not have enough energy to overcome it. Next, we observe oscillations of the kink between two curved regions. After some time, the kink stops.

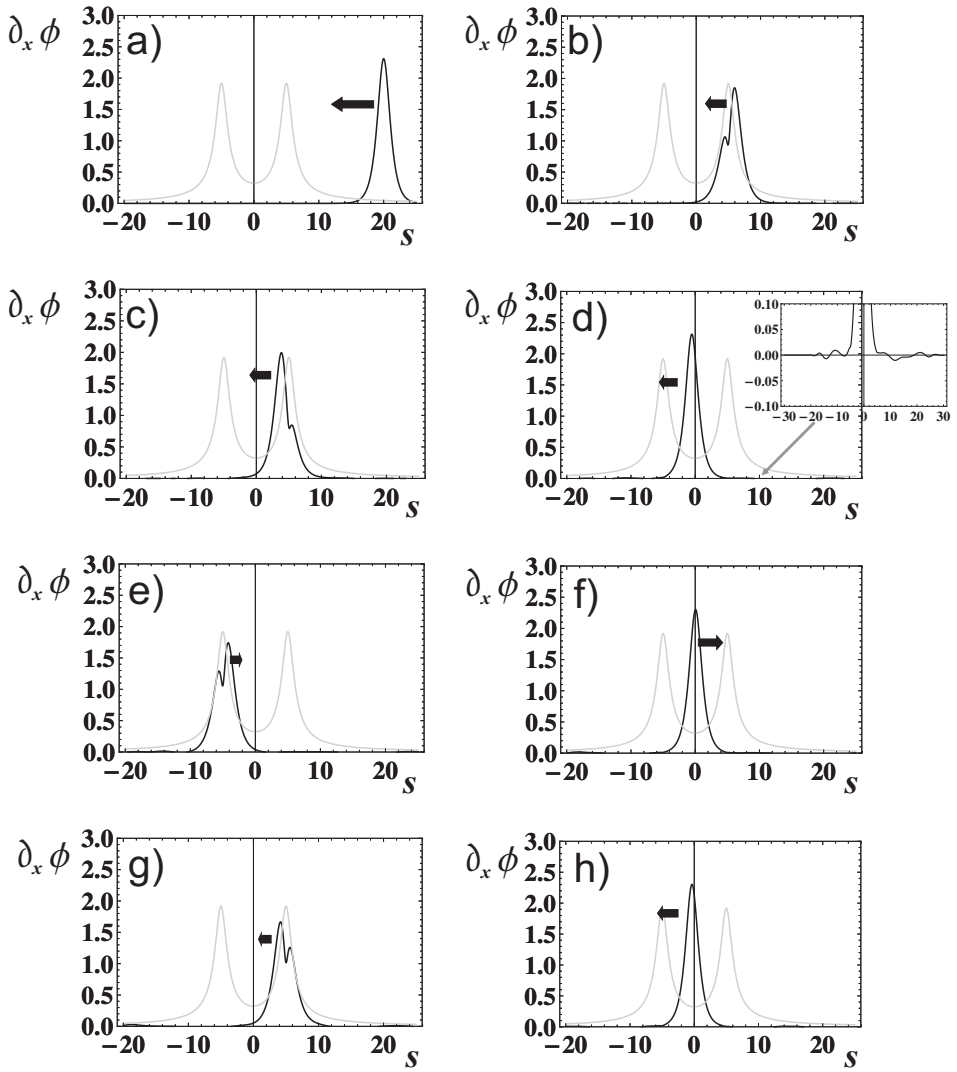

Fig. 8. The kink is confined between two curved regions of the space. The parameters of the simulation are as follows: $C = 1.86$, $v = 0.5$, $s_0 = 20$ and $l = 5$.

5. Remarks

The evolution of the kink in the curved 1d sine-Gordon model was studied in the paper [9] in the framework of the collective coordinate method. In order to use this method, one puts the kink ansatz into the Lagrangian written in curved coordinates and then integrates out all the space variables. The collective variable in the kink ansatz indicates the position of the kink.

As a result, one obtains the kinetic and potential energy of the kink in a curved space. For small curvatures, there is a simple relation between the curvature and the potential experienced by the kink.

The results of this paper have a direct application to the description of one-dimensional Josephson junctions with slowly varying curvature. The Josephson junction has possible applications in digital electronics technology. The RSFQ electronics (rapid single flux quantum) relies on quantum effects in Josephson junctions, to process digital signals. For example, if the junction is composed of two circular segments connected by a straight line, then fluxion experiences the potential of the hole in the system. The potential of this type was studied in this article (see Fig. 8) and it was shown that it can be used to store digital information in electronic devices. Furthermore, the fluxion can be extracted from this trap by the application of the external bias current.

Moreover, the collective coordinate method seems to be a good starting point to go beyond the mean field approximation. The quantum structure that stands beyond the mean field approximation can be reconstructed using the standard quantization procedure. Reconstruction of quantum energy levels is particularly interesting in the context of realization of the qubit that is a basic element of the quantum computer. The quantization can be performed by imposing the standard commutation rules between the collective coordinate and the conjugate momentum. The description of this system is given by quantum Hamiltonian.

In the present paper, we confirmed, on the background of the field model, predictions of the collective coordinate method [9]. Moreover, we found more subtle effects which are present in the regime where the collective coordinate method cannot be applied. In particular, we observed formation of the shock waves in the process of collision of ultra-fast kinks with a curved region of the space. Additionally, we explored aspects of evolution which are absent in the collective coordinate approach presented in paper [9]. An example of such a process is shown in Fig. 8 where radiation can substantially change the evolution of the system and leads to confining the kink between curved regions of space. Finally, we also proposed a simple numerical recipe for finding the kink profiles in a curved space. This recipe is based on the observation that the static sectors of the field models that differ by dissipation term are identical. Moreover, the dissipation (after a sufficiently long time) removes the kinetic energy from the system leaving only static configurations.

This work was supported in part by the National Science Center, Poland (NCN) grant 2011/03/B/ST3/00448.

REFERENCES

[1] J. Scott Russell, *Report on Waves*, Report of the Fourteenth Meeting of the British Association for the Advancement of Science, York, September 1844, p. 311, London 1845.

[2] N.J. Zabusky, M.D. Kruskal, *Phys. Rev. Lett.* **15**, 240 (1965).

[3] R. Rajaraman, *Solitons and Instantons*, North-Holland, Amsterdam 1982; M. Remoissenet, *Waves Called Solitons*, Springer, Berlin 1996.

[4] B.D. Josephson, *Adv. Phys.* **14**, 419 (1965); A. Barone, G. Paterno, *Physics and Applications of the Josephson Effect*, Wiley, New York 1982; A. Barone, F. Esposito, C.J. Magee, A.C. Scott, *Riv. Nuovo Cim.* **1**, 227 (1971); A.R. Bishop, T. Schneider, *Solitons and Condensed Matter Physics*, Berlin: Springer-Verlag, 1981; A.S. Davydov, *Solitons in Molecular Systems*, Dordrecht, The Netherlands: Reidel, 1985; J.D. Gibbon, I.N. James, I.M. Moroz, *Phys. Scr.* **20**, 402 (1979).

[5] M.J. Ablowitz, P.A. Clarkson, *Solitons, Nonlinear Evolution Equations and Inverse Scattering*, Cambridge Univ. Press, 1999; L.A. Ferreira, B. Piette, W.J. Zakrzewski, *Phys. Rev. E* **77**, 036613 (2008); S.V. Kuplevakhsky, A.M. Glukhov, *Phys. Rev. B* **73**, 024513 (2006); **76**, 174515 (2007); G. Derks, A. Doelman, S.A. van Gils, H. Susanto, *SIAM J. Appl. Dyn. Syst.* **6**, 99 (2007); J.E. Macías-Díaz, *Comput. Phys. Commun.* **181**, 1842 (2010).

[6] T. Dobrowolski, *Ann. Phys. (NY)* **327**, 1336 (2012); *J. Geom. Symmetry Phys.* **34**, 13 (2014).

[7] C. Gorria *et al.*, *Phys. Rev. B* **69**, 134506 (2004); S.V. Kuplevakhsky, A.N. Omelyanchouk, Y.S. Yerin, *Fizika Nizkikh Temperatur* **37**, 842 (2011); P.D. Shaju, V.C. Kuriakose, *Phys. Rev. B* **65**, 214508 (2002); C. Nappi *et al.*, *Phys. Rev. Lett.* **93**, 187001 (2004).

[8] J. Restrepo, R. Chitra, S. Camalet, É. Dupont, *Phys. Rev. B* **84**, 245109 (2011); S.N. Shevchenko, A.N. Omelyanchouk, E. Il'ichev, *Low Temp. Phys.* **38**, 283 (2012); S. Kawabata, S. Kashiwaya, Y. Asano, Y. Tanaka, *Physica E* **29**, 669 (2005); M. Grajcar, Yu-xi Liu, F. Nori, A.M. Zagoskin, *Phys. Rev. B* **74**, 172505 (2006); T. Shi, B. Chen, Z. Song, C.P. Sun, *Commun. Theor. Phys.* **43**, 795 (2005).

[9] T. Dobrowolski, *Phys. Rev. E* **79**, 046601 (2009); *Phys. Lett. A* **373**, 3867 (2009).

[10] V.P. Koshelets, *Supercond. Sci. Technol.* **27**, 065010 (2014) [arXiv:1312.6377v2 [cond-mat.supr-con]].

[11] W.H. Press, S.A. Teukolsky, W.T. Vetterling, B.P. Flannery, *Numerical Recipes: The Art of Scientific Computing*, Chapter 20, Cambridge University Press, Third Edition, 2007.